JCB

Supplemental material

Lu et al., https://doi.org/10.1083/jcb.201709174

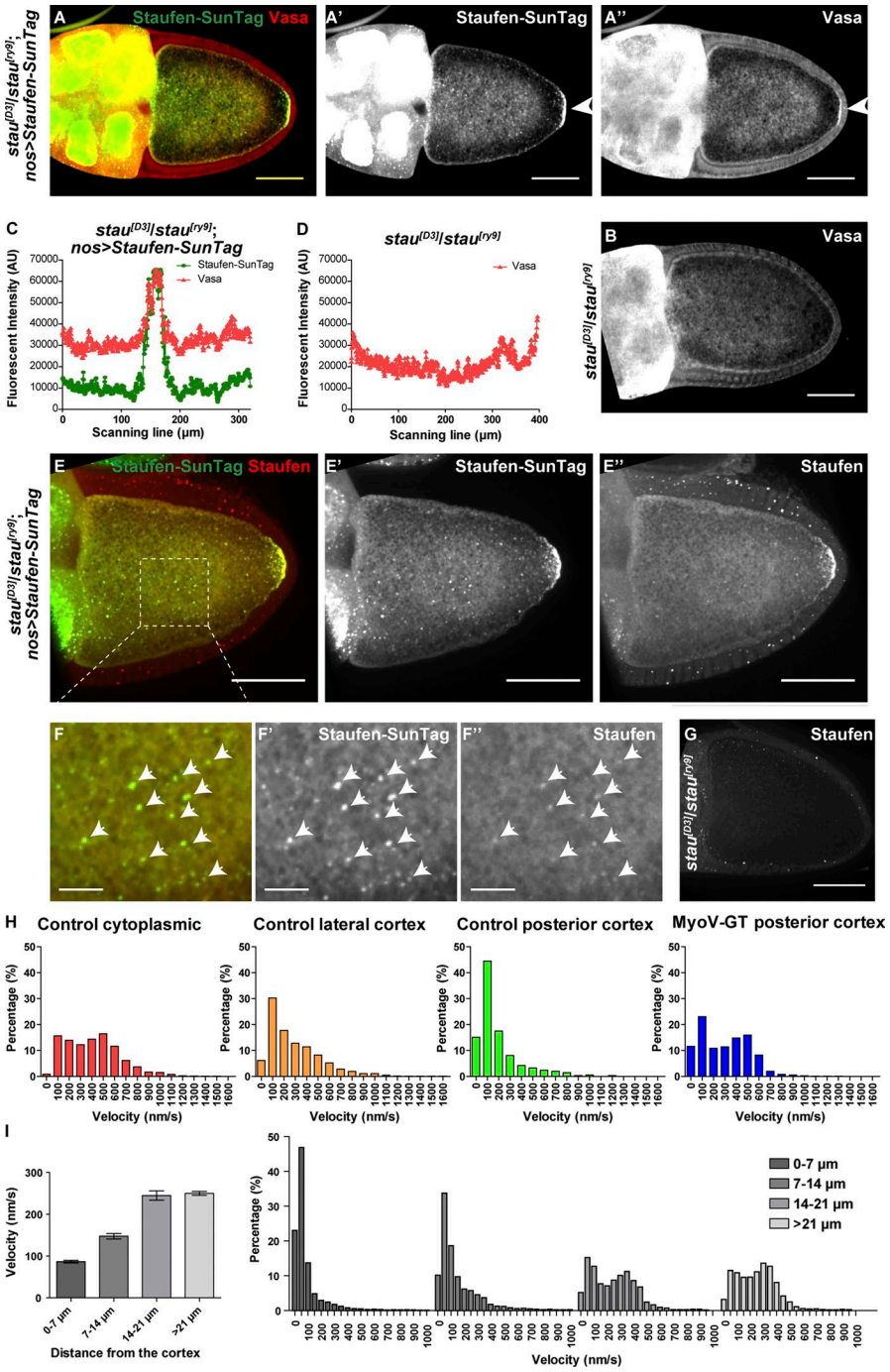

Figure S1. **Staufen-SunTag particles are functional and move at different velocities in different areas of the oocyte. (A–A'')** Staufen-SunTag in *stau*$^{[D3]}$/*stau*$^{[ry9]}$ ovaries with Vasa staining. In the absence of endogenous Staufen, Staufen-SunTag forms a tight crescent at the posterior pole of the oocyte (A', arrowhead) and recruits Vasa to the posterior pole (A'', arrowhead; *n* = 67). **(B)** No Vasa accumulation at the posterior pole in *stau*$^{[D3]}$/*stau*$^{[ry9]}$ oocytes (*n* = 72). **(C and D)** Plot profile of Staufen-SunTag and Vasa along the oocyte cortex in A and B. The fluorescent intensity peak of Vasa staining overlaps the fluorescent intensity peak of the Staufen-SunTag signal in the Staufen-SunTag–rescued *stau*$^{[D3]}$/*stau*$^{[ry9]}$ oocyte (C), whereas there is no clear peak of Vasa staining at the posterior pole in *stau*$^{[D3]}$/*stau*$^{[ry9]}$ mutant (D). **(E and F)** Staufen-SunTag in *stau*$^{[D3]}$/*stau*$^{[ry9]}$ ovaries with Staufen staining. **(E' and E'')** Individual channels of either Staufen-SunTag (E') or Staufen staining (E'') shown in E. **(F–F'')** A magnified area of E indicated by the dashed box. In the absence of endogenous Staufen, Staufen-SunTag forms a tight crescent at the posterior pole and Staufen puncta (arrowheads) in the cytoplasm of the oocyte. Both the crescent and cytoplasmic puncta are positive for Staufen staining (*n* = 30). **(G)** No Staufen staining in the *stau*$^{[D3]}$/*stau*$^{[ry9]}$ oocyte. **(H)** Histograms of Staufen-SunTag velocities in control cytoplasmic (*n* = 3,491), control lateral cortex (*n* = 2,144), control posterior cortex (*n* = 542), and *MyoV* mutant posterior cortex (*n* = 1,084). This is the same set of data as in Fig. 1 C. **(I)** Average velocities and histograms of Staufen-SunTag particles at different distances from the cortex of the posterior half of control oocytes tracked by Nikon Elements: 0–7 µm, *n* = 6,073; 7–14 µm, *n* = 2,324; 14–21 µm, *n* = 876; and >21 µm, *n* = 4,250. Bars: 50 µm (main images); 10 µm (insets).

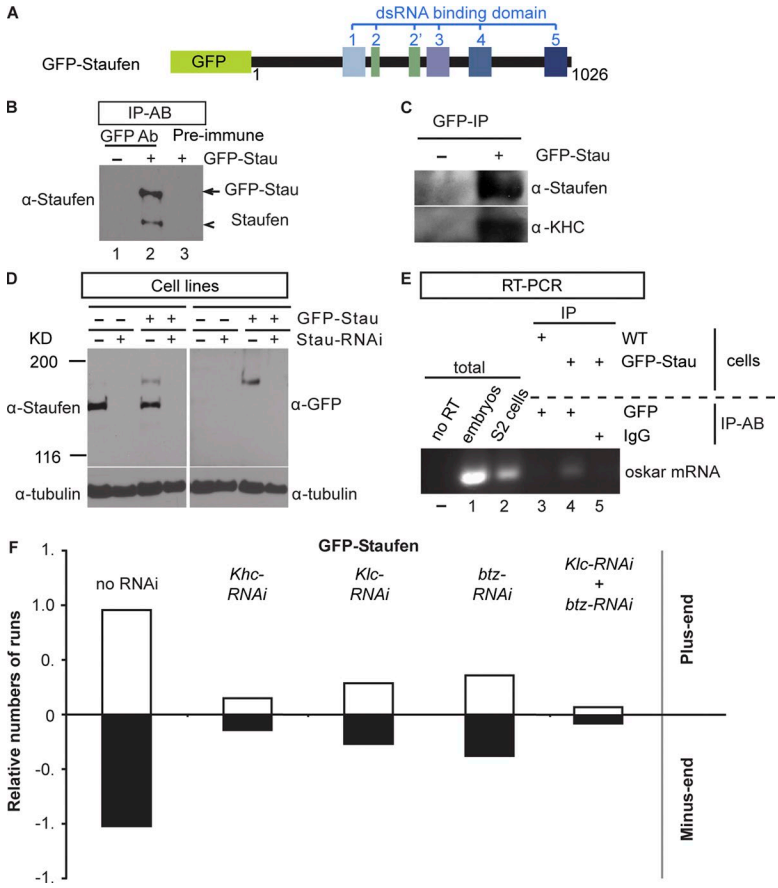

Figure S2. **GFP-Staufen forms an RNP complex in S2 cells and is transported by kinesin-1. (A)** A schematic illustration of the GFP-Staufen construct used in this study. GFP is fused to the N terminus of full-length *Drosophila* Staufen that carries five dsRNA-binding domains. **(B)** IP of GFP-Staufen pulls down the endogenous Staufen, indicating GFP-Staufen forms a complex with endogenous Staufen (lane 2). Two controls were used: (1) parental cell lines were subjected to GFP-IP (lane 1), and (2) preimmune IgG was used for GFP-Staufen cell lines (lane 3). **(C)** Staufen associates with KHC. IP using anti-GFP antibody in parental S2 (–) or stable cell lines expressing GFP-Staufen (+) showed that Staufen associates with KHC. **(D and E)** Characterization of cell lines stably expressing GFP-Staufen. **(D)** Parental S2 and GFP-Staufen cell lines were treated with or without dsRNA containing the coding region of Staufen (Stau-RNAi). Immunoblotting for Staufen confirmed that both endogenous and ectopic expression of Staufen were knocked down (KD) upon RNAi treatment. **(E)** RT-PCR of *osk* mRNA from GFP-IP in GFP-Staufen cells. no RT lane, no RT-PCR (negative control); lanes 1 and 2 are total RNA from *Drosophila* embryos, and S2 cells were used as positive control. Lanes 3 and 4 are GFP-IP from untransfected and GFP-Staufen cells, respectively. Lane 5 is rabbit IgG-IP control from GFP-Staufen cells. **(F)** Staufen uses two adaptors for kinesin-1. GFP-Staufen movement in *Khc-RNAi*, *Klc-RNAi*, *btz-RNAi*, or *Klc-RNAi* + *btz-RNAi* showed that both KLC and Btz are required for Staufen movement.

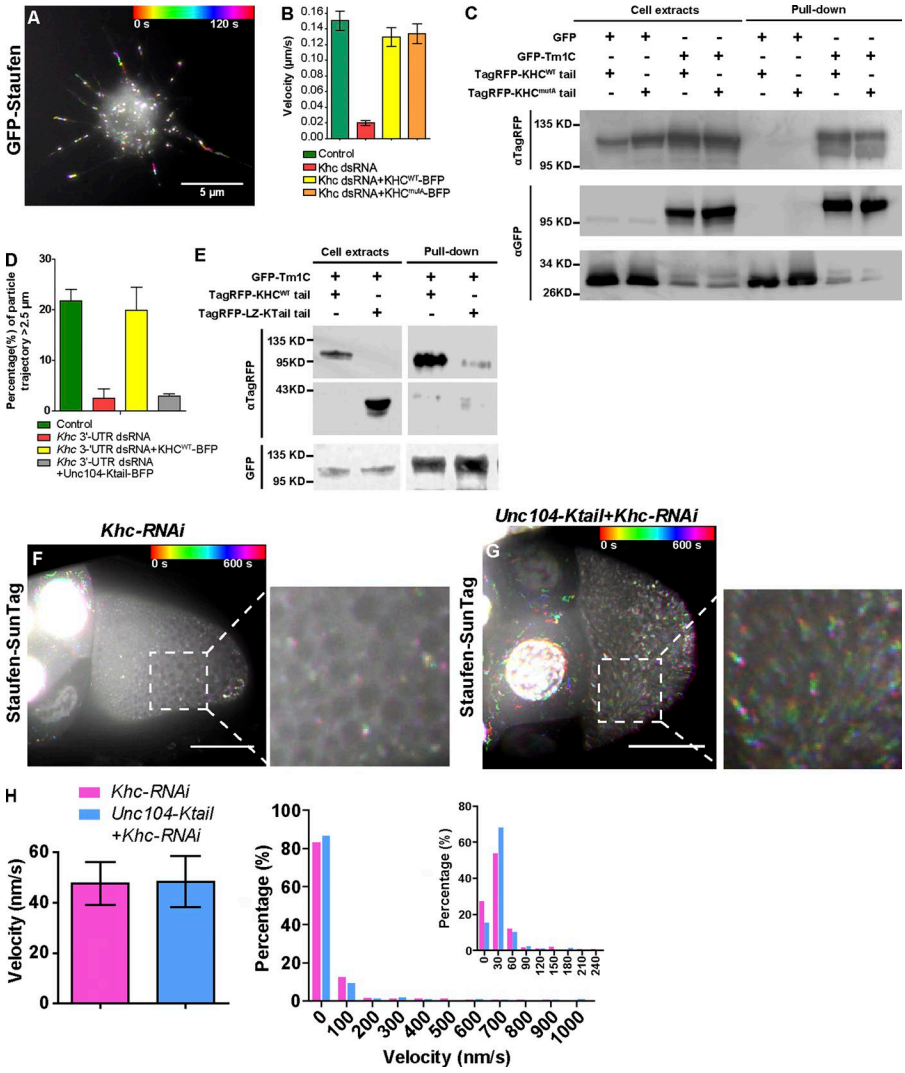

Figure S3. **KHC^{mutA} does not affect Staufen transport along microtubules, and chimeric Unc104-Ktail motor cannot transport Staufen particles.** **(A)** A temporal color-coded image of GFP-Staufen transport in an S2 cell treated with CytoD. GFP-Staufen transport is shown as rainbow tracks in the microtubule-filled processes. **(B)** Quantification of velocities (mean ± 95% confidence intervals) of GFP-Staufen in four conditions: (1) control, *n* = 962; (2) *Khc* 3′UTR-dsRNA, *n* = 221; (3) *Khc* 3′UTR-dsRNA^{+}KHC^{WT}-BFP, *n* = 1,135; and (4) *Khc* 3′UTR-dsRNA^{+}KHC^{mutA}-BFP, *n* = 771. Percentages of tracked particles with velocity >0.1 µm/s: (1) control, 37.9% (365/962); (2) *Khc* 3′UTR- dsRNA, 1.4% (3/221); (3) *Khc* 3′UTR-dsRNA^{+}KHC^{WT}-BFP, 29.4% (334/1,135); and (4) *Khc* 3′UTR-dsRNA^{+}KHC^{mutA}-BFP, 37.7% (291/771). **(C)** KHC^{mutA} tail interacts with Tm1C as efficiently as KHC^{WT} tail. GFP or GFP-Tm1C was cotransfected with either TagRFP-Khc^{WT} tail or TagRFP-Khc^{mutA} tail (without the motor domain; residues 345–975). GFP and GFP-Tm1C were pulled down by anti-GFP beads and probed with both TagRFP antibody (top) and anti-GFP antibody (bottom). **(D)** GFP-Staufen particles in S2 cells were tracked in four following conditions: (1) control (no dsRNA); (2) *Khc* 3′-UTR dsRNA; (3) *Khc* 3′-UTR dsRNA^{+}KHC-BFP (only coding region; no 3′UTR); and (4) *Khc* 3′-UTR dsRNA^{+}Unc104-Ktail-BFP. The percentage of particles with >2.5 µm trajectory was calculated as a readout of GFP-Staufen motility in S2 cells: (1) control, 21.7% (*n* = 865); (2) *Khc* 3′-UTR dsRNA, 2.6% (*n* = 270); (3) *Khc* 3′-UTR dsRNA^{+}KHC-BFP, 19.9% (*n* = 861); and (4); *Khc* 3′-UTR dsRNA^{+}Unc104-Ktail-BFP, 3.0% (*n* = 395). **(E)** The chimeric motor tail does not interact with Tm1C. GFP-Tm1C was cotransfected with either TagRFP- Khc^{WT} tail (Khc residues 345–975) or TagRFP-LZ-Ktail (leucine zipper–Ktail residues 905–975). GFP-Tm1C was pulled down by anti-GFP beads and probe with both TagRFP antibody (top) and anti-GFP antibody (bottom). **(F and H)** Chimeric Unc104-Ktail does not rescue Staufen transport along microtubules but partially rescues slow streaming in stage 9 oocytes. **(H)** Average velocities (mean ± 95% confidence intervals) and histograms of Staufen-SunTag velocities. Percentages of fast-moving particles (>100 nm/s): *Khc-RNAi*, 6.5% (34/527), and *Unc104-Ktail+Khc-RNAi*, 6.1% (25/410).

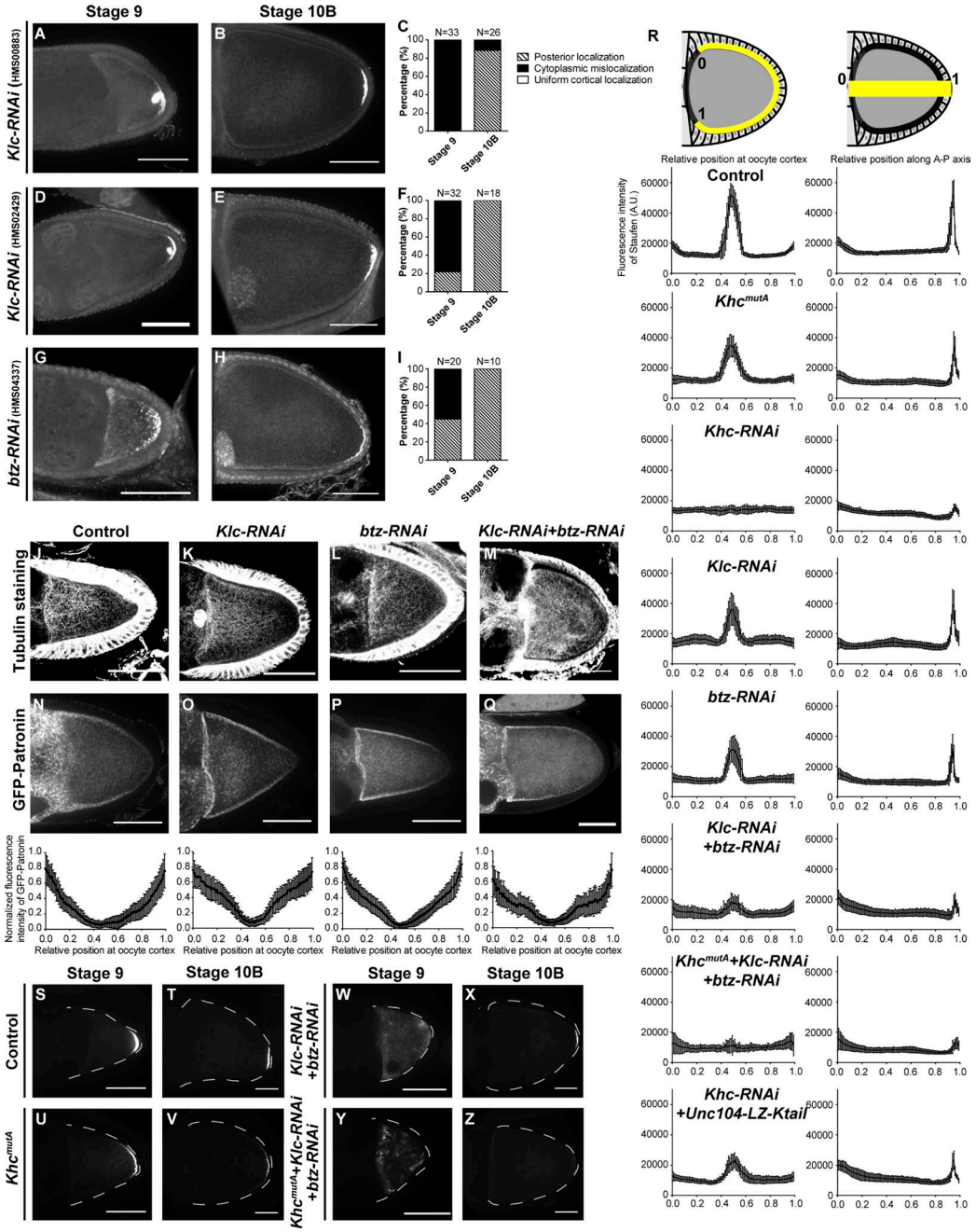

Figure S4. **Inhibition of transport only causes *osk*/Staufen mislocalization in stage 9 oocytes, while simultaneous inhibition of transport and streaming completely abolishes *osk*/Staufen posterior localization in stage 9 and stage 10B oocytes. (A–C)** Knockdown of KLC in the germ line by *Klc-TRiP RNAi-HMS00883* driven by *nos-Gal4-VP16* led to cytoplasmic mislocalization in 100% of the stage 9 oocytes (A and C) but no defects in 88.8% of the stage 10B oocytes (B and C). **(D–F)** Knockdown of KLC in the germ line by *Klc-TRiP RNAi-HMS02429* driven by *nos-Gal4-VP16* led to cytoplasmic mislocalization in 78.1% of the stage 9 oocytes (D and F) but no defects in the stage 10B oocytes (E and F). **(G–I)** Knockdown of Btz in the germ line by *btz-TRiP RNAi-HMS04337* driven by *nos-Gal4-VP16* led to cytoplasmic mislocalization in 55.0% of the stage 9 oocytes (G and I) but no defects in the stage 10B oocytes (H and I). **(J–M)** Tubulin staining in control (J), *nos>Klc-TRiP RNAi-GL00535* (K), *nos>btz-RNAi-TRiP.GLC01869* (L), and *nos>Klc-TRiP RNAi-GL00535 + btz-RNAi-TRiP.GLC01869* (M) oocytes. Images were processed using the Log function in ImageJ to show dim tubulin signal in the oocytes in the presence of the bright signal in the follicle cells. **(N–Q)** GFP-Patronin in control (N), *nos>Klc-TRiP RNAi-GL00535* (O), *nos>btz-TRiP RNAi-GLC01869* (P), and *nos>Klc-TRiP RNAi-GL00535 + btz-RNAi-TRiP.GLC01869* (Q) oocytes. Normalized GFP-Patronin signal along the cortex of the oocyte was quantified in following genotypes as a readout of the microtubule gradient: N, control, *n* = 28; O, *nos>Klc-TRiP RNAi-GL00535*, *n* = 34; P, *nos>btz-TRiP RNAi-GLC01869*, *n* = 38; and Q, *nos>Klc-TRiP RNAi-GL00535 + btz-RNAi-TRiP.GLC01869*, *n* = 30 (see the Quantification of GFP-Patronin in the oocytes section of Materials and methods for more details). **(R)** Quantification of Staufen staining along the oocyte cortex (left) and along anterior–posterior axis (right) in listed genotypes. Absolute fluorescence intensity (AU) of Staufen staining was plotted as a function of the normalized distance (illustrated as yellow lines in the cartoon from 0 to 1; see the Quantification of Staufen staining in the oocytes section of Materials and methods for more details). **(S–Z)** smFISH against *osk* mRNA in control (S, *n* = 32; T, *n* = 49), in *Khc^{mutA}* (U, *n* = 20; V, *n* = 27), *Klc* and *btz* double RNAi (W, *n* = 42; X, *n* = 53), and *Khc^{mutA}* with *Klc* and *btz* double RNAi (Y, *n* = 46; Z, *n* = 29). All the images were acquired and processed identically. Bars, 50 µm.

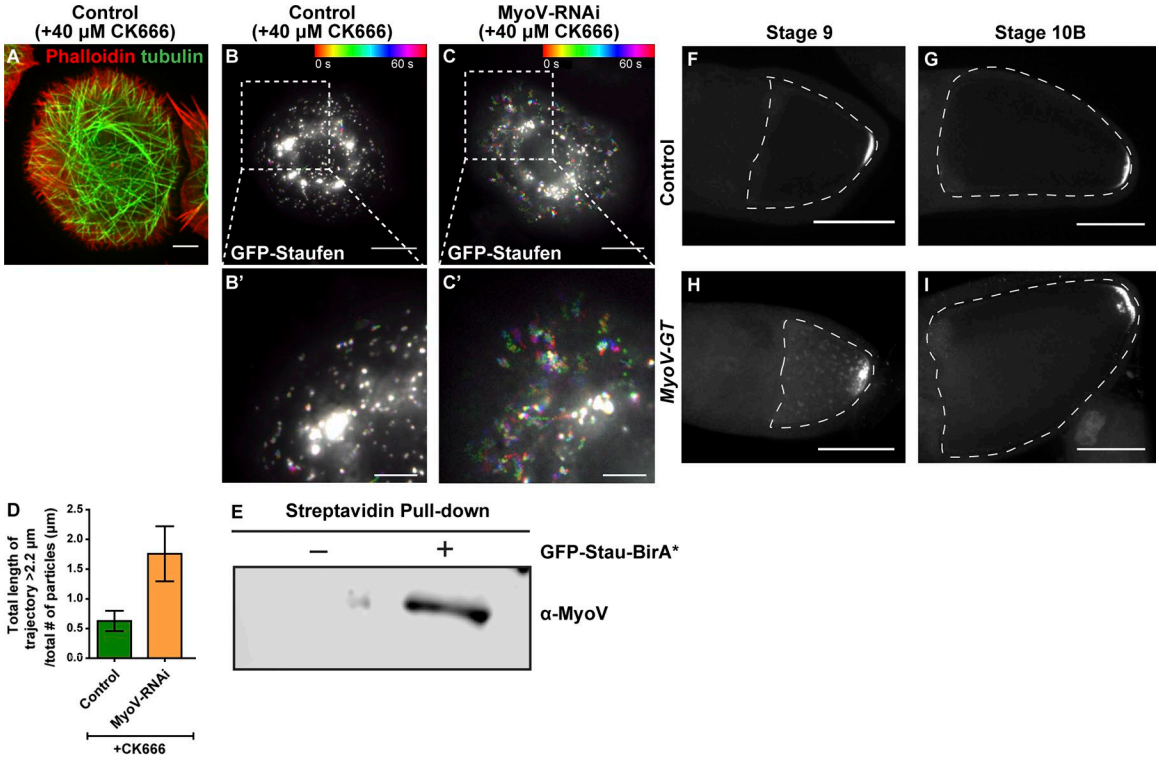

Figure S5. **MyoV functions as a local anchorage for Staufen. (A)** Microtubules (green; labeled by Dm1α tubulin staining) penetrated actin-enriched (red; labeled by rhodamine-phalloidin) lamellipodia in an S2 cell after CK666 treatment. **(B and C)** Temporal color-coded images showing GFP-Staufen movement in a control cell (B) and a MyoV-RNAi S2 cell (C). More GFP-Staufen movements (rainbow tracks) were seen in the MyoV-RNAi cells. **(B′ and C′)** A magnified area at the lamellipodia (dashed line box) of B and C. Bars: 5 µm (main images); 2 µm (insets). **(D)** Quantification of GFP-Staufen movement in control and MyoV-RNAi cells. Average trajectories (total length of trajectory >2.2 µm/total number of particles) for control cells and MyoV-RNAi cells are 0.63 ± 0.17 µm and 1.76 ± 0.46 µm (mean ± SEM), respectively. **(E)** BioID pulldown assay showed that MyoV binds to the Staufen RNP complex. *Drosophila* WT S2 cells and GFP-Stau-BirA* S2 cells were treated with biotin, lysed, pulled down by streptavidin-coated beads, and blotted against α-MyoV antibody. MyoV was only pulled down in the GFP-Stau-BirA* cells. **(F and G)** Staufen staining in control oocytes showed a compact posterior crescent at both stage 9 (F) and at stage 10B (G). **(H and I)** Ectopic expression of the dominant-negative MyoV mutant *MyoV-GT* caused Staufen mislocalization at both stage 9 and stage 10B (H, 70.6%, *n* = 17; I, 42.1%, *n* = 19). Bars, 50 µm.

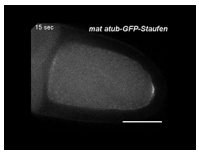

Video 1. **Staufen localization and movement in streaming oocytes.** Two representative examples of a *mat atub-GFP-Staufen* oocyte and a *nos>Staufen-SunTag* oocyte, respectively. Both GFP-Staufen and Staufen-SunTag formed posterior crescents and labeled cytoplasmic particles that were circulated with ooplasmic streaming. Both videos were imaged using identical conditions. To note, Staufen-SunTag labeling is much brighter than the GFP-Staufen. Bar, 50 µm.

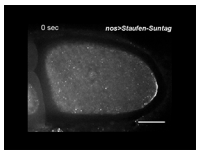

Video 2. **Streaming circulates Staufen particles to the anchorage site.** Staufen-SunTag particles were circulating along with the cytoplasmic flow and significantly slowed down near the posterior pole; some particles got incorporated into the posterior crescent. Bar, 50 µm.

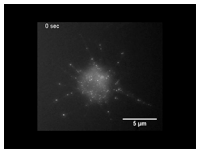

Video 3. **Staufen particles move on microtubules in S2 cells.** GFP-Staufen formed discrete particles and moved bidirectionally in the microtubule-filled processes induced by 5 µM CytoD treatment. Bar, 5 µm.

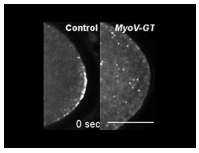

Video 4. **Inhibition of MyoV abolishes the deceleration of Staufen particles near the posterior cortex.** Distinct behaviors of Staufen-SunTag particles were observed near the posterior pole in control and *MyoV* mutant oocytes. Neither deceleration nor incorporation of Staufen-SunTag particles near the posterior pole of the oocyte with ectopic expression of *MyoV-GT* (right) compared with the control one (left). Bar, 50 µm.